Unveiling ZrO₂/natural zeolite catalytic performance on hydrocracking palm oil mill effluent residue

Junifa Layla Sihombing[1], Herlinawati[1], Ahmad Nasir Pulungan[1], Agus Kembaren[1], Gimelliya Saragih[2], Harmileni[2], Rahayu[1], Ary Anggara Wibowo[3]

[1]Department of Chemistry, Faculty of Mathematics and Natural Sciences, Universitas Negeri Medan, Medan 20221, Indonesia
[2]Politeknik Teknologi Kimia Industri, Medan 20228, Indonesia
[3]School of Engineering, College of Engineering and Computer Science, The Australian National University, North Road, 2601, Australian Capital Territory, Australia

Abstract

Palm oil mill effluent (POME) is the largest liquid waste from crude palm oil production. This liquid waste still contains a lot of chemical components, solid deposits, and oil which is dangerous if released directly into the environment. The residual oil and grease components contained in POME can be further extracted and converted into fuel fractions. This study investigates the conversion of residual oil from POME into fuel fractions through hydrocracking. A ZrO₂/Sarulla natural zeolite (SNZ) catalyst was used, characterized by a particle size of 1-1.5 μm, a surface area of 73.3 m2/g, a pore volume of 0.161 cc/g, and a pore diameter of 3.35 nm. The effect of catalyst mass was studied, with the total conversion increasing to a certain extent with increasing catalyst mass, however, an increase in coke formation decreased the product yield. The highest gasoline fraction selectivity was obtained with a catalyst mass of 0.09 wt% (~42%), while the kerosene fraction was most obtained with a catalyst mass of 0.15 wt% (~40%). The liquid product with a catalyst mass of 0.15 wt% had the highest HHV of 44.2 MJ/kg, a 12% increase from the HHV of POME oil residue (39.4 MJ/kg). The results demonstrate the potential of using residual oil from POME as a source for fuel production and the use of natural zeolite-based catalysts as hydrocracking catalysts.

Introduction

Indonesia is a leading producer of crude palm oil (CPO) on a global scale. According to the Indonesian Palm Oil Association (IPOA), in 2021, the production of CPO amounted to 46,888 million tons, yielding an export value of $35 billion, which is a 52% increase from the previous year's export value of $22.9 billion. It is projected that this production rate will continue to rise. During the palm oil production process, approximately 90% of the weight of fresh fruit bunches is discarded as waste, and only 10% is transformed into palm oil, with the rest being discarded in the form of palm oil sludge, palm fatty acid distillate, and palm oil mill effluent (POME) (Zulqarnain et al. 2021).

POME is a byproduct generated during the sterilization process of palm oil and contains substantial amounts of nutrients and phosphorus that are harmful to the environment. Pre-treatment is necessary before its discharge (Low et al. 2021). Estimates suggest that the production of CPO results in the generation of up to 3 billion pounds of POME annually (Mohammad et al. 2021). POME comprises 95-96% water, 0.6-0.7% residual oil, and 4-5% total solids, including 2-4% suspended solids (Iskandar et al. 2018; Zulqarnain et al. 2021). It has a Biological Oxygen Demand (BOD) content ranging from 25,625 to 39,616.7 mg/L and a Chemical Oxygen Demand (COD) content ranging from 117,333.3 to 146,333.3 mg/L, presenting serious environmental hazards (Leela et al. 2018). The Total Suspended Solids (TSS) content ranges from 5000 to 54,000 mg/L, and oil and grease ranges

from 130 to 18,000 mg/L (Mohammad et al. 2021; Ng et al. 2019). If POME is discharged directly into the ground, it causes groundwater stagnation and damages the surrounding vegetation. Its discharge into waterways leads to water depletion and pollution, putting aquatic life at risk from residual oil. Currently, pond systems or land application techniques are widely used for treating POME before discharge into the environment (Mohammad et al. 2021). However, this method demands a large area for waste storage and a considerable time for the liquid waste to meet the government's wastewater quality standards. Moreover, the oil layer in POME can reduce the effectiveness of conventional biological pond systems, as it surrounds the suspended microbes (Semilin et al. 2021). The residual oil in POME has the potential to be converted into biodiesel feedstock. This raw material is considered low-grade oil with high free fatty acid content but is abundant and cost-effective. Based on estimates of the 3 billion pounds of POME produced annually, the extractable oil and grease are projected to reach approximately 9,500 tons per year.

Previous efforts have been made to convert residual oil from palm oil mill effluent (POME) into fuel fractions. Davies et al. (2022) converted fatty acids from POME to biodiesel using H_2SO_4 as a catalyst and obtained the highest yield of 89% at 150°C for 15 minutes. However, homogeneous catalysts can complicate product separation and cause corrosion. Hence, heterogeneous catalysts are preferred for their ease of separation and reusability. Hasanudin and Rachmat (2016) esterified the extracted oil from POME with a heterogeneous composite catalyst of tungsten and zirconium oxide at a catalyst concentration of 10% with a methanol-to-oil ratio of 8:1 at 70°C for 2 hours, achieving a maximum conversion of 74.88%. Muanruksa et al. (2021) used a Pd/Al_2O_3 catalyst to hydrocrack fatty acids from POME and obtained a biofuel yield of 94% with a biojet fraction selectivity of 57.44% at 400°C for 1 hour. Although the conversion of POME into biodiesel fractions has been well documented, the cracking process into light fuel fractions, including gasoline and kerosene, using heterogeneous catalysts is still limited.

This study aims to obtain the light fraction of fuel through hydrocracking extracted oil from POME using a heterogeneous catalyst based on natural zeolite from Sarulla, North Sumatra. The catalyst has been modified by embedding ZrO_2 metal oxide to enhance its performance. Natural zeolite is a promising catalyst material due to its abundant availability and potential to reduce production costs. Moreover, the natural zeolite from Sarulla has been reported to possess superior characteristics, such as a large surface area, good porosity, modifiable acidity, and good thermal resistance at high temperatures, which make it suitable for catalytic cracking reactions (Gea et al. 2022; Sihombing et al. 2020). The combination of metal oxide active sites and Brønsted and Lewis acid sites from the zeolite support is expected to exhibit synergistic effects in the catalytic cracking of extracted oil from POME. Additionally, variations of the catalyst mass were investigated to optimize the catalytic performance and selectivity.

Method

Materials
The palm oil mill effluent (POME) was collected from the PTKI Medan mini palm oil mill. The reagents used in this study included distilled water, double distilled water (DDW), natural zeolite sourced from Sarulla (North Sumatra, Indonesia), $ZrCl_4$, HCl, H_2SO_4, H_3PO_4, n-hexane, methanol, and NaOH obtained from Merck (Darmstadt, Germany). Hydrogen, oxygen, and nitrogen gases were supplied by PT. Aneka Gas (Medan, Indonesia).

Palm Oil Mill Effluent Preparation
The process of obtaining oil from POME involved heating the POME at 105°C to evaporate the water, followed by filtering to separate the mixed solids. Degumming was performed to separate phosphatides, proteins and resins by adding a solution of 0.6% phosphoric acid (H_3PO_4) in the amount of 1-3% of the volume of POME. The oil-grease extraction process was carried out using n-hexane as the solvent with a 1:0.8 ratio of n-hexane to POME. The mixture was then sonicated for 5 minutes, transferred to a separatory funnel, and allowed to separate into two layers for 15 minutes. The top layer was evaporated to obtain a thick oil extract from POME. The extract was then heated at 105°C for 45 minutes to remove the remaining solvent. After drying, the oil was placed in a desiccator and the oil recovery was calculated using equation:

$$\text{Yield (mg/L)} = \frac{\text{Weight Dry Oil Content (mg) x 1000}}{\text{Sample Volume (L)}}$$

Preparation and Activation of Sarulla Natural Zeolite

The procedure for the preparation and activation of natural zeolite in this study was based on the method reported by Sihombing et al. (2018). The first step involved crushing and sieving the natural zeolite to obtain a particle size that passed through a 100 mesh sieve. The zeolite was then subjected to 24 hours of immersion in distilled water at room temperature, followed by filtration and drying at 100 °C. The activation of the zeolite was performed using 3M HCl at a temperature of 90 °C for 30 minutes. The sample was filtered, and the precipitate was washed with distilled water until a neutral pH was achieved. The filtered precipitate was dried at 120 °C for 3 hours. Finally, the sample was subjected to calcination at a temperature of 500 °C in a nitrogen gas flow to produce the acid-activated natural zeolite (SNZ).

Preparation of ZrO2/SNZ Catalyst

The preparation of ZrO_2-loaded natural zeolite (ZrO_2/SNZ) in this study was conducted following the procedure outlined by Pulungan et al. (2021), using the wet impregnation method followed by oxidation. ZrCl4 was dissolved in double distilled water (DDW) and added to a predetermined amount of acid-activated natural zeolite (SNZ). The mixture was placed in a three-neck flask and heated at 90°C for 4 hours. The resulting product was dried at 120°C, and then calcined at 500°C for 1 hour under nitrogen (N_2) flow, followed by oxidation at the same temperature with oxygen (O_2) for 1 hour to obtain the ZrO_2/SNZ catalyst.

Catalyst Characterization

The crystalline properties of the catalyst were analyzed using X-Ray Diffractometry (XRD) on a Shimadzu 6100 instrument with Cu Kα (λ = 1.54184 Å) radiation at 40kV and 30 mA, covering a range of 2θ values from 7.00 to 70.00°. The surface morphology, elemental composition, and mapping of the catalyst were investigated through Scanning Electron Microscopy (SEM) on a Zeiss EPOMH 10Zss device equipped with Energy Dispersion X-Ray Spectroscopy (EDX). Nitrogen gas adsorption-desorption isotherm analysis was performed using a Gas Sorption Analyzer (NOVA 1200e) from Quantachrome at 77 K. The specific surface area was determined using the Brunauer-Emmett-Teller (BET) method and the volume and pore diameter based on the Barret-Joyner-Halenda (BJH) model.
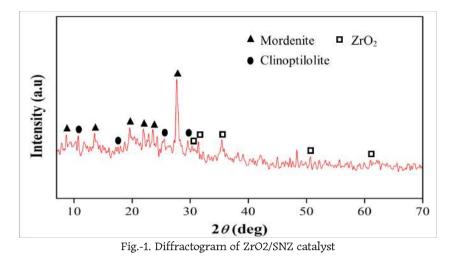
Hydrocracking of Extracted Oil from POME

The hydrocracking process was performed in a fixed-bed reactor with a diameter of 5.5 cm and a height of 25 cm. The catalyst vessel had a diameter of 4.8 cm and a height of 3.5 cm, while the furnace was 40 cm in diameter and 39 cm in height. The experiment utilized POME oil with catalyst masses of 0.09, 0.12, and 0.15 wt.% that were heated at 500 °C in a temperature-controlled heating flask for 2 h. The resulting cracked oil vapor was cooled and condensed, and the condensed liquid was analyzed qualitatively via Gas Chromatography Mass Spectrophotometry (GC-MS) to determine the carbon chain and type of biofuel produced. The Higher Heating Value (HHV) was determined using a Bomb Calorimeter.

Results and Discussion

Catalyst Crystallinity

The phase and mineral/metal composition of the material were determined through X-Ray Diffraction (XRD) analysis. The XRD measurement was conducted within the 2θ range of 7 to 70 degrees, and the resulting diffractogram is presented in Fig.-1.

Based on the diffractogram in Fig.-1, peak characteristics for natural zeolite are observed in the range of 2θ = 9-30°. In diffractogram patterns, several peaks appearing at 9.9°, 13.6°, 19.6, 22.4°, 25.6°, and 27.7° are characteristic of mordenite (JCPDS file 5–0490). Meanwhile, the peaks observed at 11.2°, 17.3°, 26.3°, and 30.0° fit with the corresponding data of clinoptilolite (JCPDS file 25–1349). This proves that the types of minerals contained in the natural zeolite used are mordenite and clinoptilolite. These results are in accordance with data reported by Wahyuni et al. (2022) which states that natural zeolite from Yogyakarta, Indonesia is composed of clinoptilolite and mordenite as its main components. In addition, the ZrO_2 peak was observed with a low

Fig.-1. Diffractogram of ZrO2/SNZ catalyst

intensity due to the small amount. Characteristic peaks for ZrO_2 appeared at 28.1°, 31.5°, 34.1°, and 35.3° (JCPDS #88-2390) indicating the presence of monoclinic ZrO_2, whereas at 30.3°, 35.2°, 50.6°, and 60.1° (JCPDS #80-2155) indicates the ZrO_2 tetragonal phase. These peaks are also in a good agreement with previous study data reported by Huang et al. (2021).

Morphology and Composition of Catalyst

The surface morphology of the catalyst was analyzed using a Scanning Electron Microscopy (SEM) with 5000x magnification, as depicted in Fig.-2a. Meanwhile, the particle size distribution is shown in Fig.-2b. The particle size distribution exhibits a relatively homogeneous range between 1-1.5 µm. However, the surface of the ZrO_2/SNZ catalyst reveals variations in particle size and the presence of significant agglomerates. This is believed to be a result of sintering and agglomeration that occur at elevated temperatures during the calcination process.
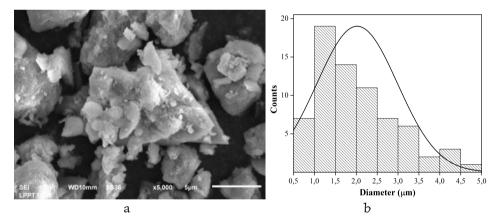

Fig.-2. (a) Surface morphology of ZrO2/SNZ catalyst at 5000 times magnification and (b) Catalyst particle size distribution

The chemical composition of the catalyst was analyzed through Energy Dispersive X-ray Spectroscopy (EDX) and confirmed through Elemental Mapping using SEM-Mapping. The results are summarized in Table 1. The findings of the study by Gea et al. (2020) were used as a comparison for the SNZ catalyst prior to the addition of metal oxides. After being loaded with metal oxides, the ZrO_2/SNZ catalyst displayed several compositional changes, including an increase in the percentage of Si, Al, and the appearance of Zr metal. The mapping results depicted in Fig.-3. reveal that the catalyst is predominantly composed of Si and Al, as represented by intense red and blue colors, respectively. Zr, represented by green, displays a less intense color due to its lower amount. The Zr content was found to be 0.63%, which was less than the added mass by 1%. It is speculated that some Zr was lost during the process or not present on the surface of the catalyst, but instead, distributed in its pores.

Moreover, the increased percentage of Si and Al leads to an increase in the Si/Al molar ratio from 2.68 to 3.10. This increase in the Si/Al ratio corresponds to an increase in acid density and results in the

hydrophobicity of the catalyst (da Costa-Serra et al. 2020; Wang et al. 2019). The increase in Si/Al ratio is indicated due to acid treatment in the natural zeolite activation process.

Table 1. Composition and ratio of Si/Al of SNZ and ZrO$_2$/SNZ catalysts

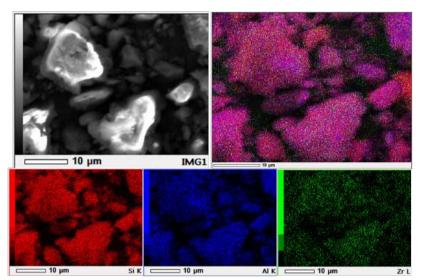| Composition (Mass %)	SNZ[a]	ZrO$_2$/SNZ
Si	15.7	25.3
O	61.6	50.6
Al	5.64	7.84
Zr	0.00	0.63
Si/Al	2.68	3.10

Fig.-3. SEM-EDX elemental mapping of the ZrO$_2$/SNZ catalyst. The distribution of elements shows different color for aluminum with red color, silicon with blue color, and zirconium with green color.

This is in accordance with a study reported by Wang et al. (2019) which states that the acid treatment of natural zeolite causes an increase of SiO$_2$/Al$_2$O$_3$ ratio where there is a decrease of polar Si-O-Al group, thereby increasing hydrophobicity (water vapour adsorption from 0.9359 mg/m2 into < 0.3077 mg/m2). Catalysts with elevated hydrophobicity are better suited for catalyzing nonpolar samples. Additionally, a higher Si/Al ratio increases the thermal resistance of the catalyst at elevated reaction temperatures.

N$_2$ Gas Sorption Analysis

The surface area and pore characteristics of the catalyst were analyzed using the N$_2$ gas adsorption-desorption phenomenon. The resulting isotherm graph, shown in Fig.-4. displays a hysteresis loop at a relative pressure of 0.4-0.9, which is characterized as type IV based on IUPAC classification and represents mesopore materials (Sotomayor et al. 2018). Further analysis was conducted by calculating the surface area through the BET method and the pore size using the BJH model, as summarized in Table 2.

Table 2. Surface area, pore volume, and pore diameter of the catalyst

Catalyst	Surface area (m^2/g)	Pore volume (cc/g)	Pore diameter (nm)
SNZ[a]	59.6	0.150	3.44
ZrO$_2$/SNZ	73.3	0.161	3.35

Table 2 illustrates differences in both the surface area and pore characteristics after the ZrO$_2$ metal oxide was embedded. The impregnation, calcination, and oxidation processes led to an increase in surface area and pore volume, and a decrease in pore diameter. The pore size of the 3.35 nm catalyst corresponds to the indication of the isotherm shape, which characterizes mesopore materials in the size range of 2-50 nm. This is also supported by the pore size distribution data in Fig.-5. which shows that the dominant pore size ranges from 10-40 Å (1-4 nm).

The increase in surface area was likely caused by the calcination and oxidation processes, carried out at high temperatures using N$_2$ and O$_2$ gases, respectively, which removed impurities from the surface of the catalyst.

This resulted in an open and cleaner surface and pores. The surface area of ZrO_2/SNZ in this study was higher than that obtained in the previous study by Pulungan et al. (2021) of 27.57 m2/g. This value is also relatively higher than the surface area of natural zeolite which is loaded with metal oxides Fe_2O_3, ZnO, and CuO of 12.9, 50.3, and 30.7 m2/g respectively (Sihombing et al. 2023). The larger surface area improves the catalyst's performance by facilitating the reactants' adsorption process and providing access to the active site. Additionally, the smaller pore diameter but increased volume may be due to the presence of metal oxides, which distribute the embedded metal throughout the catalyst pores, narrowing the pore diameter but encouraging the expansion of the pores inward, resulting in a larger pore volume.
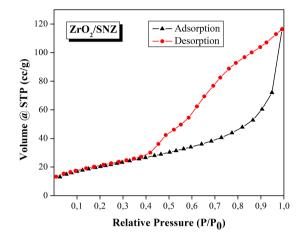

Fig.-4. Graph of N_2 gas adsorption-desorption isotherm on ZrO_2/SNZ catalysts.
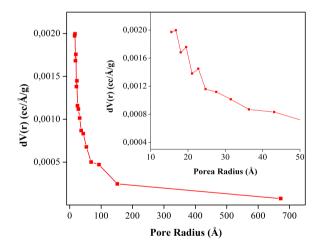

Fig.-5. Pore size distribution of ZrO2/SNZ catalyst

Oil Extraction from POME

Residual oil was extracted from POME using n-hexane as solvent via soxhlet extraction, a cost-effective method for oil recovery. Compared to ethanol, toluene, and methanol solvents, n-hexane has the highest oil recovery from POME with an oil extraction yield of 90% achieved (Zulqarnain et al. 2021). In this study, the extracted oil was 9923 mg/L. The oil yield depends on the initial state of POME and extraction process. GC-MS analysis of the oil revealed the main fatty acid components: palmitic acid (39.57%), oleic acid (38.45%), and linoleic acid (10.82%) with minor amounts of stearic acid (4.67%), lauric acid (2.47%), myristic acid (1.7%), arachidic acid (0.34%), and linolenic acid (0.22%). These results align with those reported who found palmitic acid (63%), oleic acid (17.4%), and other fatty acids as the main components in residual oil from POME (Hasanudin et al. 2012).

Product Distribution

The ZrO_2/SNZ catalyst, with superior characteristics compared to SNZ without metal oxides, was used for the hydrocracking of POME oil at 500℃. The reaction was carried out using 0.09 wt%, 0.12 wt%, and 0.15 wt% of ZrO2/SNZ catalyst. Figure 6. shows that the catalyst mass affects the product yield (Hasanudin et al. 2022). The

catalyst increases reaction rate towards equilibrium and decreases the amount of unconverted oil in the reactor, requiring a suitable mass for complete conversion. However, more catalyst results in more coke, a deactivation factor in oil hydrocracking. The number of active sites, affecting the rate of coke formation, also increases with catalyst mass.
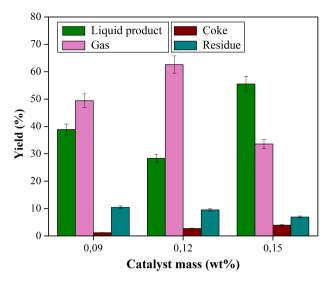

Fig.-6. Distribution of POME Hydrocracking products using a ZrO_2/SNZ catalyst with a catalyst mass of 0.09, 0.12, and 0.15 wt%.

The oil cracking reaction produces liquid and gaseous products. The catalyst:oil ratio affects product distribution. A higher catalyst amount facilitates a more frequent catalytic reaction. The reaction with 0.15 wt% ZrO_2/SNZ catalyst yielded the most liquid product (~56%) and the least gas (32%). The reaction with 0.12 wt% ZrO_2/SNZ catalyst produced almost 30% liquid product and over 60% gas. Meanwhile, the reaction with 0.09 wt% ZrO_2/SNZ catalyst yielded liquid and gaseous products of similar amounts (40% and 50% respectively) with no significant difference.

Biofuel Fraction Selectivity

The resulting liquid product was tested for its content using GC-MS analysis. The liquid product content is grouped based on the amount of carbon into the gasoline fraction (C5-C11), the kerosene fraction (C12-C15), and the diesel fraction (C16-C20). The selectivity of the resulting liquid products is summarized in Fig.-7.
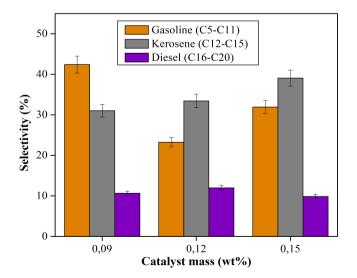

Fig.-7. Selectivity of liquid products for gasoline, kerosene and diesel fractions

Figure 7. demonstrates that the highest selectivity for gasoline fraction was achieved for the product catalyzed by ZrO_2/SNZ 0.09 wt% (~42%) and the lowest for the product catalyzed by ZrO_2/SNZ 0.12 wt% (~24%).

In contrast, the maximum kerosene fraction was obtained from the 0.15 wt% ZrO_2/SNZ catalyst (~40%) and the minimum from the 0.09 wt% ZrO_2/SNZ catalyst (~30%). The selectivity for diesel fraction remained almost unchanged among the three products.

The variation in the distribution of the fractions produced is correlated with the process of breaking large molecular bonds into smaller molecules. ZrO_2/SNZ 0.12 wt% catalyst produces the minimum gasoline fraction but the maximum gas product. This suggests that a significant amount of bond breaking occurs, resulting in the production of the most gas molecules. On the other hand, ZrO_2/SNZ catalyst has a relatively large surface area compared to zeolite without ZrO_2, facilitating the catalytic reaction on the catalyst surface. Additionally, deep meso-sized pores form, which trap molecular bulk to be cleaved during the hydrocracking reaction. Hence, the addition of the ZrO_2/SNZ catalyst mass also impacts the availability of active sites and the process of breaking long chain oil molecules into light fractions.
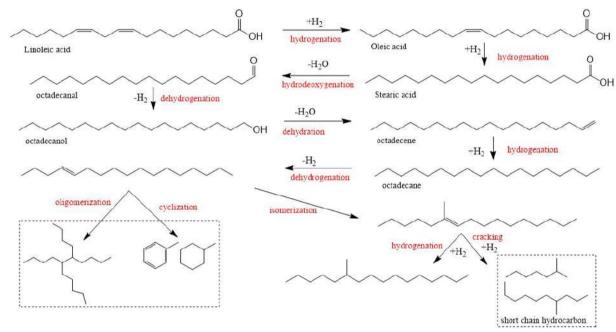

Fig.-8. Proposed reaction pathway for the transformation of linoleic acid

The addition of the catalyst mass should be carried out judiciously, as excessive use results in more coke formation, which is unavoidable during the hydrocracking process. This coke can obstruct the active sites of the catalyst and fill the pores, reducing the rate of cleavage reaction and hence, the production of light fractions. This was observed at the catalyst mass of 0.15 wt%, where the most coke was formed, leading to lower gasoline fraction and higher kerosene production.

The mechanism of breaking long-chain molecular bonds during the hydrocracking reaction can be investigated through analyzing the components present in the POME oil residue and the resulting liquid product. Fig.-8, depicts the proposed mechanism that may occur. As depicted in Fig.-8, linoleic acid, the main fatty acid component, undergoes various pathways to produce short-chain compounds. Initially, linoleic acid undergoes a hydrogenation reaction, where H+ attacks the C=C bond to form oleic acid. Further hydrogenation results in the formation of stearic acid (Puello-Polo et al. 2022). Stearic acid, a saturated chain, undergoes hydrodeoxygenation, releasing its hydroxyl group as a water molecule to form an aldehyde group. This aldehyde is converted into an alcohol compound through a dehydrogenation process and then undergoes dehydration to form an alkene compound (Duongbia et al. 2022). The alkene can take multiple pathways, including hydrogenation and oligomerization and cyclization, with hydrogenation resulting in the formation of alkanes, which can further crack into short-chain hydrocarbon molecules as the end-product of the hydrocracking reaction. Meanwhile, further oligomerization and cyclization of alkenes leads to the formation of coke-forming molecules (Žula et al. 2022).

Catalysts play a crucial role in facilitating various pathways in hydrocracking reactions. The ZrO_2/SNZ catalyst contains a Brønsted acid site from zeolite and an active site ZrO_2 metal oxide. Ideal cracking occurs on a bifunctional catalyst with a sufficient number of Brønsted acid sites to facilitate the hydrogenation reaction.

Table 3. Calorific values extracted oil from POME and hydrocracking liquid products

Sample	HHV (MJ/kg)
Extracted oil from POME	39.4
ZrO_2/SNZ 0.09 wt.%	43.3
ZrO_2/SNZ 0.12 wt.%	43.0
ZrO_2/SNZ 0.15 wt.%	44.2

The mechanism involves dehydrogenation of branched alkanes, followed by bond breaking, hydrogenation, and desorption of the two molecules from the catalyst surface. ZrO_2, being oxophilic, tends to promote direct HDO reactions (Žula et al. 2022). In addition to the active site factor, material characteristics such as porosity, particle size, and surface area also impact the catalytic activity of the catalyst.

Calorific Value

The higher heating value (HHV) of the resulting liquid product was analyzed. The results are summarized in Table 3. The HHV of the residual oil extracted from POME was found to be 39.4 MJ/kg, and after undergoing the hydrocracking process, this value increased by 12% to 44.2 MJ/kg in the liquid product catalyzed by ZrO_2/SNZ 0.15 wt%.

Conclusion

POME residue oil was extracted, yielding an extract of 9923 mg/L with main fatty acids including 39.57% palmitic acid (C16), 38.45% oleic acid (C18:1C-1), and 10.82% linoleic acid (C18:2C). The hydrocracking reaction utilized ZrO_2/SNZ catalyst with particle size 1-1.5 μm, surface area 73.3 m2/g, pore volume 0.161 cc/g, and pore diameter 3.35 nm. Results showed increasing catalyst mass increases total conversion to a limit, but also increases coke formation and reduces product. The ZrO_2/SNZ catalyst broke long chain fatty acid molecules to produce light fuel fractions through hydrogenation, dehydrogenation and cracking. The gasoline fraction showed the highest selectivity of ~42% with ZrO_2/SNZ 0.09 wt%, while the kerosene fraction was obtained the most from ZrO_2/SNZ 0.15 wt% by ~40%. The liquid product from ZrO_2/SNZ 0.15 wt% had the highest HHV of 44.2 MJ/kg, a 12% increase from POME oil residue's 39.4 MJ/kg. These results show the potential for oil residue from POME to be converted into fuel fractions, thus there is a great opportunity to process the oil losses into value-added chemicals. Meanwhile, apart from its abundant potential availability and unique characteristics, the development of the use of natural zeolite-based catalysts needs to be optimized to obtain better product selectivity.

Conflict of Interests

The author (s) declares that there is no conflict of interest in this research and manuscript.

Acknowledgements

References

da Costa-Serra, J. F., Cerdá-Moreno, C., & Chica, A. (2020). Zeolite-supported Ni catalysts for CO2 methanation: Effect of zeolite structure and Si/Al ratio. *Applied Sciences* (Switzerland), 10(15). https://doi.org/10.3390/app10155131

Davies, E., Deutz, P., & Zein, S. H. (2022). Single-step extraction–esterification process to produce biodiesel from palm oil mill effluent (POME) using microwave heating: a circular economy approach to making use of a difficult waste product. *Biomass Conversion and Biorefinery*, 12(7), 2901–2911. https://doi.org/10.1007/s13399-020-00856-1

Duongbia, N., Kannari, N., Sato, K., Takarada, T., & Chaiklangmuang, S. (2022). Production of bio-based chemicals from palmitic acid by catalytic hydrotreating over low-cost Ni/LY char and limonite catalysts. *Alexandria Engineering Journal*, 61(4), 3105–3124. https://doi.org/10.1016/j.aej.2021.08.037

Gea, S., Haryono, A., Andriayani, A., & Sihombing, J. L. (2020). The stabilization of liquid smoke through hydrodeoxygenation over nickel catalyst loaded on Sarulla natural zeolite. *Applied Sciences*, 10, 1–17.

Gea, S., Irvan, I., Wijaya, K., Nadia, A., Pulungan, A. N., Sihombing, J. L., & Rahayu, R. (2022). Bio-oil hydrodeoxygenation over acid activated-zeolite with different Si/Al ratio. *Biofuel Research Journal*, 9(2), 1630–1639. https://doi.org/10.18331/brj2022.9.2.4

Hasanudin, H., Putri, Q. U., Agustina, T. E., & Hadiah, F. (2022). Esterification of free fatty acid in palm oil mill effluent ussulfated carbon-zeolite composite catalyst. *Pertanika Journal of Science and Technology*, 30(1), 377–395. https://doi.org/10.47836/pjst.30.1.21

Hasanudin, H., & Rachmat, A. (2016). Production of biodiesel from esterification of oil recovered from palm oil mill effluent (POME) sludge using tungstated-zirconia composite catalyst. *Indonesian Journal of Fundamental and Applied Chemistry*, 1(2), 42–46. https://doi.org/10.24845/ijfac.v1.i2.42

Hasanudin, Said, M., Faizal, M., Dahlan, M. H., & Wijaya, K. (2012). Hydrocracking of oil residue from palm oil mill effluent to biofuel. *Sustainable Environment Research*, 22(6), 395–400.

Huang, C., Zhu, C., Zhang, M., Lu, Y., Wang, Q., Qian, H., Chen, J., & Fang, K. (2021). Direct Conversion of Syngas to Higher Alcohols over a CuCoAl|t-ZrO2 multifunctional catalyst. *ChemCatChem*, 13(13), 3184–3197. https://doi.org/10.1002/cctc.202100293

Iskandar, M. J., Baharum, A., Anuar, F. H., & Othaman, R. (2018). Palm oil industry in South East Asia and the effluent treatment technology—A review. *Environmental Technology and Innovation*, 9(May 2017), 169–185. https://doi.org/10.1016/j.eti.2017.11.003

Leela, D., Nur, S. M., Yandri, E., & Ariati, R. (2018). Performance of Palm Oil Mill Effluent (POME) as biodiesel source based on different ponds. *E3S Web of Conferences*, 67, 1–9. https://doi.org/10.1051/e3sconf/20186702038

Low, S. S., Bong, K. X., Mubashir, M., Cheng, C. K., Lam, M. K., Lim, J. W., Ho, Y. C., Lee, K. T., Munawaroh, H. S. H., & Show, P. L. (2021). Microalgae cultivation in palm oil mill effluent (Pome) treatment and biofuel production. *Sustainability* (Switzerland), 13(6). https://doi.org/10.3390/su13063247

Mohammad, S., Baidurah, S., Kobayashi, T., Ismail, N., & Leh, C. P. (2021). Palm oil mill effluent treatment processes—A review. *Processes*, 9(5), 1–22. https://doi.org/10.3390/pr9050739

Muanruksa, P., Winterburn, J., & Kaewkannetra, P. (2021). Biojet Fuel Production from Waste of Palm Oil Mill Effluent through Enzymatic Hydrolysis and Decarboxylation. *Catalysts*, 11(1). https://doi.org/10.3390/catal11010078

Ng, K. H., Yuan, L. S., Cheng, C. K., Chen, K., & Fang, C. (2019). TiO2 and ZnO photocatalytic treatment of palm oil mill effluent (POME) and feasibility of renewable energy generation: A short review. *Journal of Cleaner Production*, 233, 209–225. https://doi.org/10.1016/j.jclepro.2019.06.044

Puello-Polo, E., Arias, D., & Márquez, E. (2022). Al2O3-MgO Supported Ni, Mo, and NiMo mixed phosphidic-sulphidic phase for hydrotreating of stearic and oleic acids into green diesel. *Frontiers in Chemistry*, 10(May), 1–18. https://doi.org/10.3389/fchem.2022.880051

Pulungan, A. N., Kembaren, A., Nurfajriani, N., Syuhada, F. A., Sihombing, J. L., Yusuf, M., & Rahayu, R. (2021). Biodiesel production from rubber seed oil using natural zeolite supported metal oxide catalysts. *Polish Journal of Environmental Studies*, 30(6), 5681–5689. https://doi.org/10.15244/pjoes/135615

Semilin, V., Janaun, J., Chung, C. H., Touhami, D., Haywood, S. K., Chong, K. P., Yaser, A. Z., & Zein, S. H. (2021). Recovery of oil from palm oil mill effluent using polypropylene micro/nanofiber. *Journal of Hazardous Materials*, 404(PB), 124144. https://doi.org/10.1016/j.jhazmat.2020.124144

Sihombing, J. L., Gea, S., Pulungan, A. N., Agusnar, H., Wirjosentono, B., & Hutapea, Y. A. (2018). The characterization of Sarulla natural zeolite crystal and its morphological structure. *AIP Conference Proceedings*, 2049. https://doi.org/10.1063/1.5082467

Sihombing, J. L., Gea, S., Wirjosentono, B., Agusnar, H., Pulungan, A. N., Herlinawati, H., & Yusuf, M. (2020). Characteristic and catalytic performance of Co and Co-Mo Metal Impregnated in Sarulla Natural Zeolite Catalyst for hydrocracking of MEFA rubber seed oil into biogasoline fraction. *Catalysts*, 10, 121.

Sihombing, J. L., Herlinawati, H., Pulungan, A. N., Simatupang, L., Rahayu, R., & Wibowo, A. A. (2023). Effective hydrodeoxygenation bio-oil via natural zeolite supported transition metal oxide catalyst. *Arabian Journal of Chemistry*, 16(6), 104707. https://doi.org/10.1016/j.arabjc.2023.104707

Sotomayor, F., Quantatec, A. P., Sotomayor, F. J., Cychosz, K. A., & Thommes, M. (2018). Characterization of micro/mesoporous materials by physisorption: Concepts and case studies. *Acc. Mater. Surf. Res*, 3(2), 34–50. https://www.researchgate.net/publication/331260891

Wahyuni, E. T., Diantariani, N. P., Kartini, I., & Kuncaka, A. (2022). Enhancement of the photostability and visible photoactivity of ZnO photocatalyst used for reduction of Cr(VI) ions. *Results in Engineering*, 13, 100351. https://doi.org/https://doi.org/10.1016/j.rineng.2022.100351

Wang, C., Leng, S., Guo, H., Yu, J., Li, W., Cao, L., & Huang, J. (2019). Quantitative arrangement of Si/Al ratio of natural zeolite using acid treatment. *Applied Surface Science*, 498(May), 143874. https://doi.org/10.1016/j.apsusc.2019.143874

Žula, M., Grilc, M., & Likozar, B. (2022). Hydrocracking, hydrogenation and hydro-deoxygenation of fatty acids, esters and glycerides: Mechanisms, kinetics and transport phenomena. *Chemical Engineering Journal*, 444(February). https://doi.org/10.1016/j.cej.2022.136564

Zulqarnain, Yusoff, M. H. M., Ayoub, M., Hamza Nazir, M., Zahid, I., Ameen, M., Abbas, W., Shoparwe, N. F., & Abbas, N. (2021). Comprehensive review on biodiesel production from palm oil mill effluent. *ChemBioEng Reviews*, 8(5), 439–462. https://doi.org/10.1002/cben.202100007

Zulqarnain, Yusoff, M. H. M., Ayoub, M., Nazir, M. H., Sher, F., Zahid, I., & Ameen, M. (2021). Solvent extraction and performance analysis of residual palm oil for biodiesel production: Experimental and simulation study. *Journal of Environmental Chemical Engineering*, 9(4), 105519. https://doi.org/10.1016/j.jece.2021.105519